J Oceanogr (2011) 67:613–625
DOI 10.1007/s10872-011-0061-0

ORIGINAL ARTICLE

Amplification of semidiurnal internal tide observed in the outer part of Tokyo Bay

Yujiro Kitade · Yosuke Igeta · Ryohei Fujii · Mitsuhiro Ishii

Received: 26 January 2011 / Revised: 31 May 2011 / Accepted: 8 July 2011 / Published online: 10 August 2011

Abstract Monitoring using a thermistor array and an acoustic Doppler current profiler was carried out in the outer part of Tokyo Bay from May 20 to November 30, 2006. Current fluctuations with tidal periods were amplified during the maximum temperature period in early September. The strong current interfered with fishing operations using set nets. Although the current fluctuation was speculated to be baroclinic motion from a phase relationship among fluctuations of temperature, current and sea level, empirical orthogonal function analysis showed the dominance of a barotropic structure. Such a discrepancy in the current structure was explained by an internal tide propagating along a deep canyon in the outer part of Tokyo Bay. Furthermore, amplification of the semidiurnal internal tide and the warming of the temperature field were found to be induced by the intrusion of Kuroshio warm water. The amplification mechanism was examined using a two-dimensional model with idealized topography. It was concluded that the large amplitude of the semidiurnal internal tide is resonantly generated in the deep canyon in the outer Tokyo Bay when stratification becomes strong and the period of the internal seiche approaches the semidiurnal period.

Keywords Internal tide · Tokyo Bay · Internal seiche · Resonance · Monitoring

Y. Kitade (✉)
Department of Ocean Sciences, Tokyo University of Marine Science and Technology, Konan 4-5-7, Minato-ku, Tokyo 108-8477, Japan
e-mail: ykitade@kaiyodai.ac.jp

Y. Igeta
Japan Sea National Fisheries Research Institute, Fisheries Research Agency, 1-5939-22 Suido-cho, Chuo-ku, Niigata-city, Niigata, Japan

R. Fujii
Canon IT Solutions Inc., Tokyo, Japan

M. Ishii
Chiba Prefectural Fisheries Research Center, Chiba, Japan

1 Introduction

Tokyo Bay is enclosed by the Boso and Miura peninsulas (Fig. 1). Topographically, the inner and outer parts of Tokyo Bay are connected by a narrow channel between the Futtsu-misaki and Kannon-zaki capes. While the inner part of Tokyo Bay is shallow with an average water depth of 20 m, a deep canyon with an average water depth of about 500 m exists in the outer part of the bay. The canyon extends from north to south and is connected by a deep trough in Sagami Bay.The physical processes in the inner part of Tokyo Bay have many times been discussed separately from the outer part of Tokyo Bay (e.g., Guo and Yanagi 1998; Radjawane et al. 2001). However, the oceanographic processes and the water mass in the inner part of Tokyo Bay are influenced by the oceanic conditions of the outer bay (e.g., Fujiwara and Yamada 2002). Furthermore, temperature and current fluctuations in the outer bay are strongly affected by the variation of the Kuroshio axis and coastal-trapped waves (Ishidoya et al. 2006; Kitade and Matsuyama 2000). Thus, the outer part of Tokyo Bay is considered the boundary between the estuary and the ocean.

The outer part of Tokyo Bay is an important fishing area. Set nets are used to catch migratory fish. The operation of pulling up a set net becomes difficult when the current is greater than 0.4 m s^{-1}. Fishing by a set net is

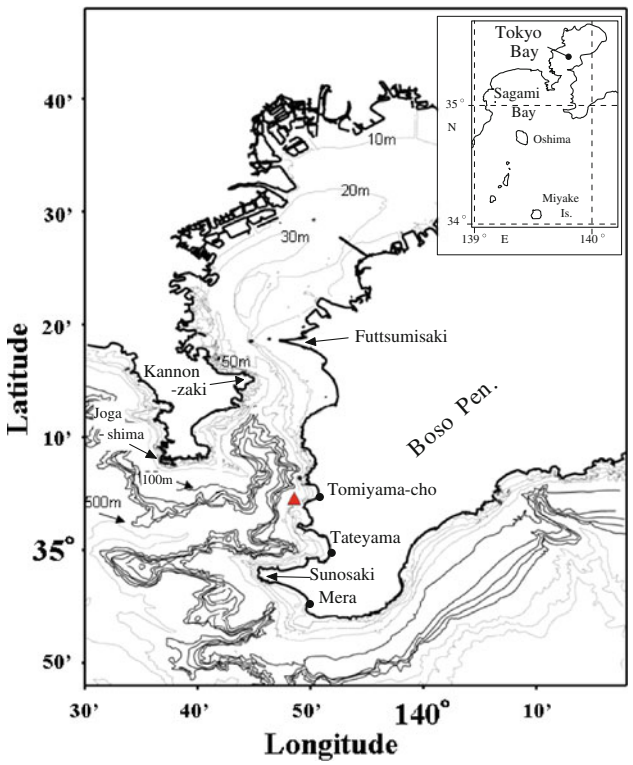

Fig. 1 Bottom topography in and around of Tokyo Bay. The monitoring station is indicated by the *filled triangle*. Intervals of bottom contour lines are 10 m from 10 to 50 m, 100 m from 100 to 500 m, and 500 m for deeper than 1,000 m. *Inset* the location of Tokyo Bay

carried out when the tidal current is weak, such as during the conversion current period between flood tide and ebb tide. However, in this area, the tidal current does not stop during the conversion current period but is still strong in the lower layer during the period of weak surface current. Such irregularities in the tidal fluctuations have interfered with fishing by set nets in the outer Tokyo Bay. Matsuyama and Iwata (1985) reported a similar problem related to tidal currents in Sagami Bay. They reported that the current is induced by the internal tide. Thus, it is possible that the strong irregular current arising in the outer part of Tokyo Bay is also related to the internal tide.

Matsuyama et al. (1992) reported that the internal tides are occasionally amplified and cause serious damage to the fishing set nets in Sagami Bay. Based on mooring observations at seven stations in the bay and a numerical model, Kitade and Matsuyama (1997) showed that the semidiurnal internal tides are generated not only at the northern part of Izu Ridge but also at the shallow region around the south of Boso Peninsula. They reported that these semidiurnal internal tides propagate into Sagami Bay and outer Tokyo Bay as an internal Poincaré wave, and interfere with the reflected waves. Such an interference of the semidiurnal internal tide would generate a strong current and cause a large displacement of the thermocline along the coast of the bay. Although interference and local enhancement of internal tides are also expected in the outer part of Tokyo Bay, it is difficult to elucidate the behavior of the internal tides because no long-term mooring data are available that describe the current variations and density fields.

In order to clarify the characteristics of current in the outer part of Tokyo Bay, we monitored temperature and current for a 6-month period. We discovered an event, that is, significantly amplified current fluctuations with the semidiurnal period during the period at the maximum water temperature. The purposes of this paper are to describe the characteristics of the current associated with internal tides and to clarify a mechanism of the significantly amplified current fluctuations observed in the outer part of Tokyo Bay.

2 Observations and data

Real-time observation using a monitoring system, float-type E-monitor (Nichiyu Giken Kogyo), was performed from May 20 to November 30, 2006, at about 1 km off Tomiyama-cho, in the eastern area of outer Tokyo Bay (Fig. 1; water depth of the monitoring point is 45 m). The monitoring system consists of two parts: a data sampling part which measures temperature and current velocity in sea water, and a telecommunication part on the surface buoy which sends the measured data by a personal digital cellular telecommunication system (NTT-docomo). Figure 2 shows the two buoys moored by a 25-mm rope at the base of the southern end of a set net. From these buoys, temperature data were obtained by a thermistor array at six layers (5, 10, 15, 20, 30, and 40 m depths) at 10-min intervals. Current data were obtained by an acoustic Doppler current profiler (ADCP) (Work-horse 300 kHz; Teledyne RDI) at 18 layers below 4 m depth at 30-min intervals. A solar battery was used for temperature measurement and telecommunication, whereas power for the ADCP operation was supplied by an internal battery. To conserve power, temperature and ADCP data were archived and sent once a day. During the monitoring period, current data at depths lower than 20 m could not be obtained because of a decrease in acoustical power caused by organisms adhering to the transducer. After cleaning the transducer, current data at depths deeper than 20 m were again obtained normally. Current data were good for more than 60% of this study. In this monitoring system, lack of temperature and current data were also caused by the bad condition of the telecommunications. If the period in which data were not available was shorter than 6 h, then data for that period were interpolated using data from the previous and subsequent periods. Compass magnetic correction was applied to all current data.

In addition to the monitoring data, sea level data obtained at Mera and Miyake Island and wind speed data obtained at Oshima were used in this study. Sea level data were obtained from the Japan Oceanographic Data Center. Wind and barometric data were obtained from the Japan Meteorological Agency. The hourly barometric data were obtained at Tateyama and Miyake Island and were used to eliminate the barometric effects from the sea level data at Mera and Miyake Island, respectively.

3 Variation of temperature and current

Figure 3 shows time variations of temperature and current at the monitoring station, sea level at Mera, and wind speed at Oshima Island. Both current components (eastward and northward) oscillated in a similar periodical way throughout the observation period. Comparing the sea level data and current fluctuations, the current appeared to oscillate with the tidal period. Although the oscillation was occasionally amplified, it was not always amplified during the spring tide. This result indicates that the current oscillations are not due to the barotropic tide. A significant amplification of the current oscillation was found from the end of August to the middle of September, during the maximum temperature period. During the same period, temperature fluctuations were amplified only in the lower layer, indicating a deepening of the thermocline depth. After the abrupt temperature rise, the temperature fluctuations were seen occasionally in the lower layer and the amplitudes of the current oscillation were larger than before the event in all three layers. Fishing using set net had stopped during the period of strong current oscillation in the early September.

Figure 4 shows time variations of the vertical structures of temperature and the eastward current with sea level fluctuation in representative three periods with different stratification conditions: period I, June 16–25; period II, September 19–28; and period III, November 1–10. Semidiurnal fluctuations were dominant in all three periods, and vertical displacements of temperature contour occasionally exceed 10 m. In period I, deepening of the temperature contours was accompanied by the eastward current in the upper layer, and the phases of temperature and current fluctuations were slightly delayed in the lower layer. In periods II and III, temperature fluctuations sometimes appeared in the middle and lower layers, and the deepening of the temperature contour was accompanied by an eastward current throughout the water column. From the comparison of sea level and current fluctuations, we can see that current is not always strong in the period of large surface displacement and does not keep the same phase relationship with surface displacement throughout the period. These properties imply that the current are not directly related to the surface tide. Vertical displacement of the temperature contour agreed with that of sea level in the phase relationship, whereas its amplitude is much larger than that of surface displacement.

Although the vertical structure of current is like a barotropic wave in periods II and III, current and temperature fluctuations are expected to be due to internal tide.

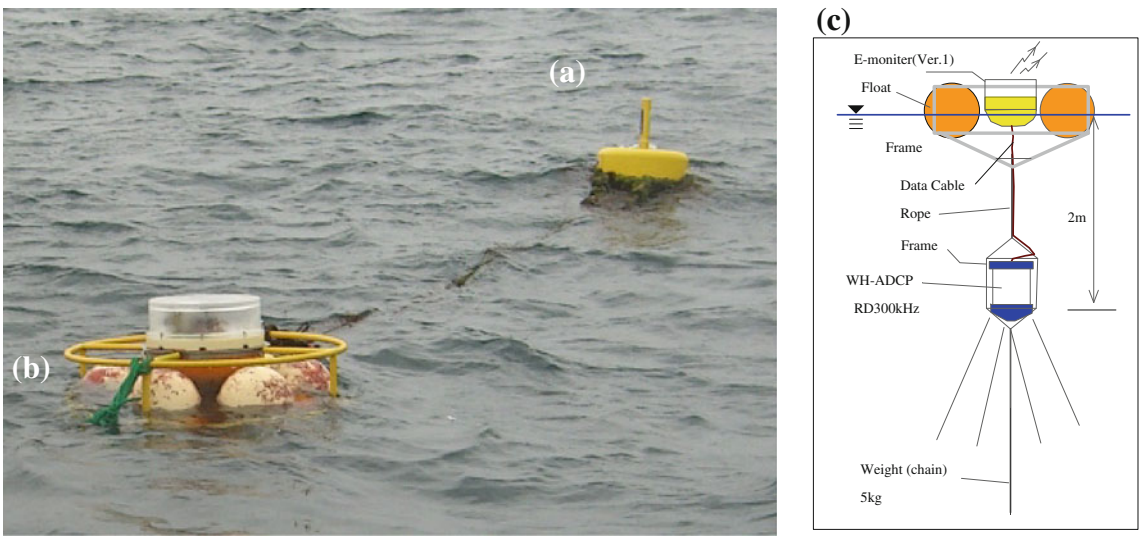

Fig. 2 Picture of monitoring system. Temperature data were obtained by **a** buoy system with thermistor array and current data were obtained by **b** buoy system with ADCP. **c** Schematic views of the buoy system with ADCP

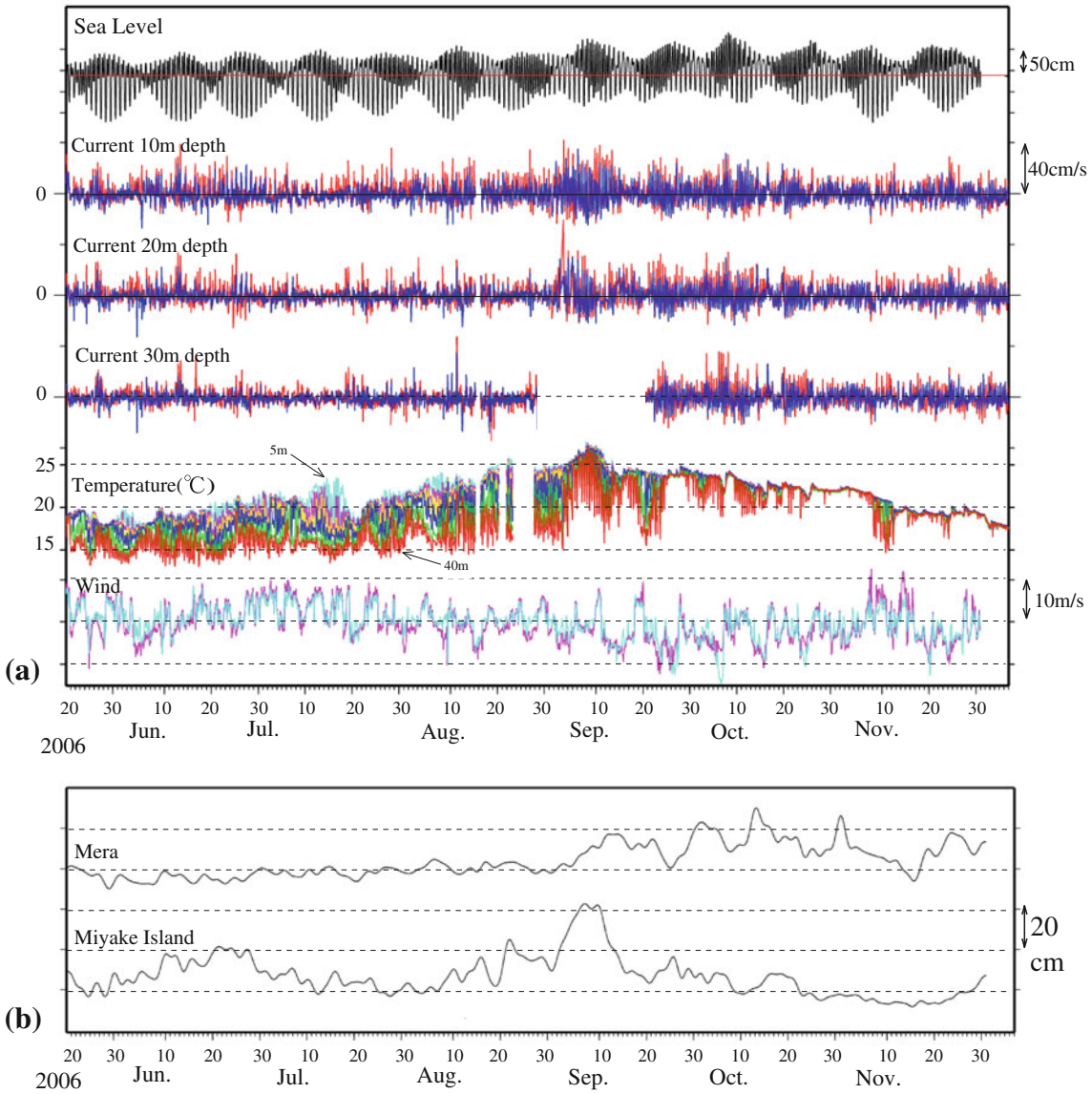

Fig. 3 **a** Time series of sea level (*black*), current components (*red* eastward component, *blue* northward component), temperature (*light blue* 5 m, *pink* 10 m, *yellow* 15, *blue* 20, *green* 30 m, *red* 40 m) and wind (*pink* eastward component, *light blue* northward component). Temperature and current data were filtered by a 2-h running average. **b** Time series of sea level at Mera and Miyake Island. The sea level data were adjusted by removing the barometric effect and by eliminating the tidal components

4 Analysis

4.1 Predominant periods of temperature and current fluctuations

Dominant periods were detected for the eastward and northward currents, temperature by spectral analysis. Figure 5 shows the power spectra calculated for three periods: period I, June 16–30; period II, September 1–15; period III, November 1–15. The data from September 1 to 15 were used in this spectral analysis for period II, because of significant amplification of current. The power spectra of the current components and temperature indicate that the semidiurnal period is most dominant in all three periods, and the energy level of the semidiurnal peak is one order of magnitude larger in period II than in the other periods. Comparing the energy levels of the semidiurnal peak, the energy levels of both current components decreased with depth in period I. Power spectra in period II and III show that the spectral structure for semidiurnal frequency band was almost the same for both current components. Since energy levels of the diurnal period band were almost the same in all three period, we can say that the amplification of current oscillations in the early September as shown in Fig. 3 was induced by the amplification of semidiurnal period band.

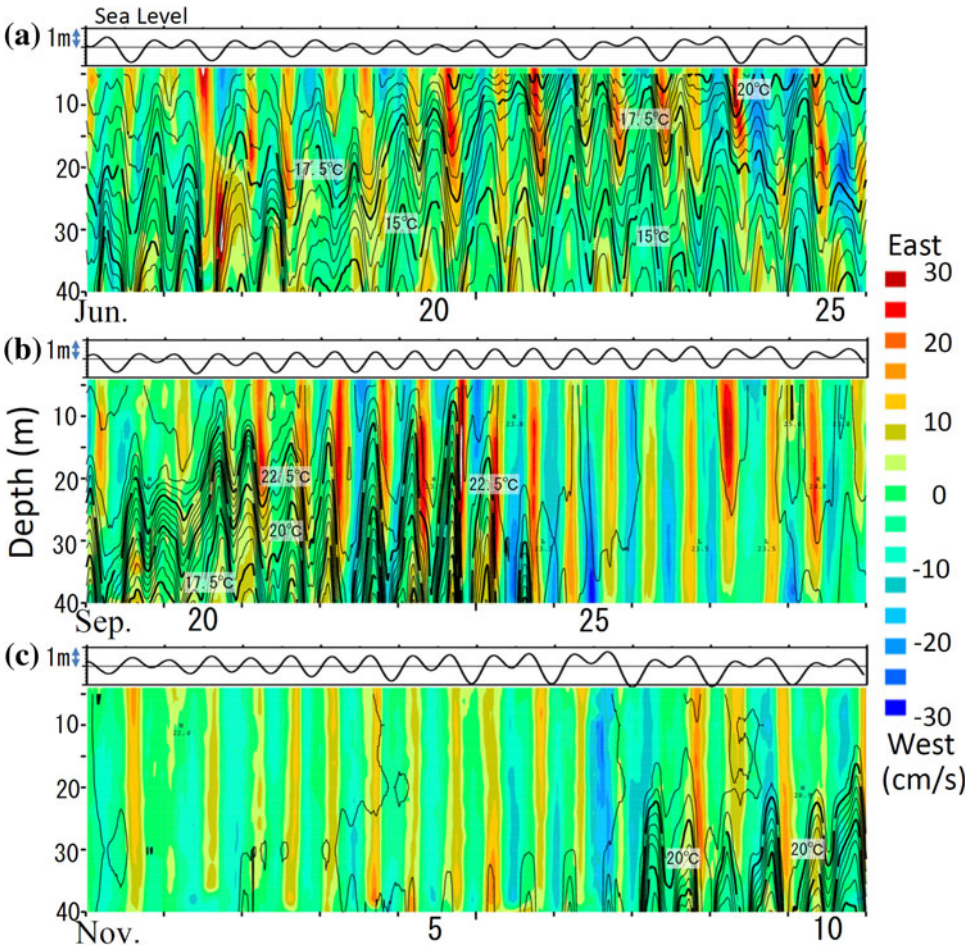

Fig. 4 Fluctuation of the eastward component of current (*color*) and temperature (*contour*) during **a** June 16–25, **b** September 19–28, **c** November 1–10. Contour interval of temperature is 0.5°C. Time variation of sea level at Mera is indicated in the *upper panel* of each figure

In addition, it is interesting that the energy peak of diurnal period has been found in both fluctuations in temperature and current for all three periods, although the diurnal internal tide was not observed in Sagami Bay (Ohwaki et al. 1994). This observation supports the results of the numerical model by Kitade and Matsuyama (1997), which shows that the diurnal internal tide generated in the shallow region around the southern part of Boso Peninsula propagated to the outer part of Tokyo Bay.

4.2 Variations of energy level and phase relation for the semidiurnal period fluctuations

Daily variations of the energy level for the semidiurnal current fluctuations were obtained for all periods by applying spectral analysis to 3 days of data. Daily variations of the coherence and phase difference for the combinations of sea level and current, sea level and temperature, and temperature and current, were also estimated by using 3 days of data. The analyses used current data at 10 m and 18 m depths, temperature data at 30 m depth, and sea level data. Figure 6 shows the relationship over time between the phase difference and energy level for the semidiurnal period. The figure shows the phase relationships with coherence larger than confidence level of 95%.

Energy density for the semidiurnal current was found to fluctuate with a period of spring and neap tidal cycles, and the energy level abruptly increased at the beginning of September and gradually decreased with time after mid-October. The phase differences between the eastward current and sea level fluctuated around 150° in June. In this analysis, a phase difference of 150° implies that the sea level displacement leads the eastward current by about 5 h. In August, the phase difference between the current and sea level decreased to 90° for the eastward current and 60° for the northward current. In early September, the phase difference was almost zero when the energy level of the current oscillation was at the maximum. Thereafter, the phase difference fluctuated around 0°.

The phase difference between temperature and both current components fluctuated around −60° in June (i.e., northeastward current leads the temperature increase by about 2 h), and they changed to −90° in September. The phase difference between the temperature and sea level gradually decreased with time; that is, the difference was

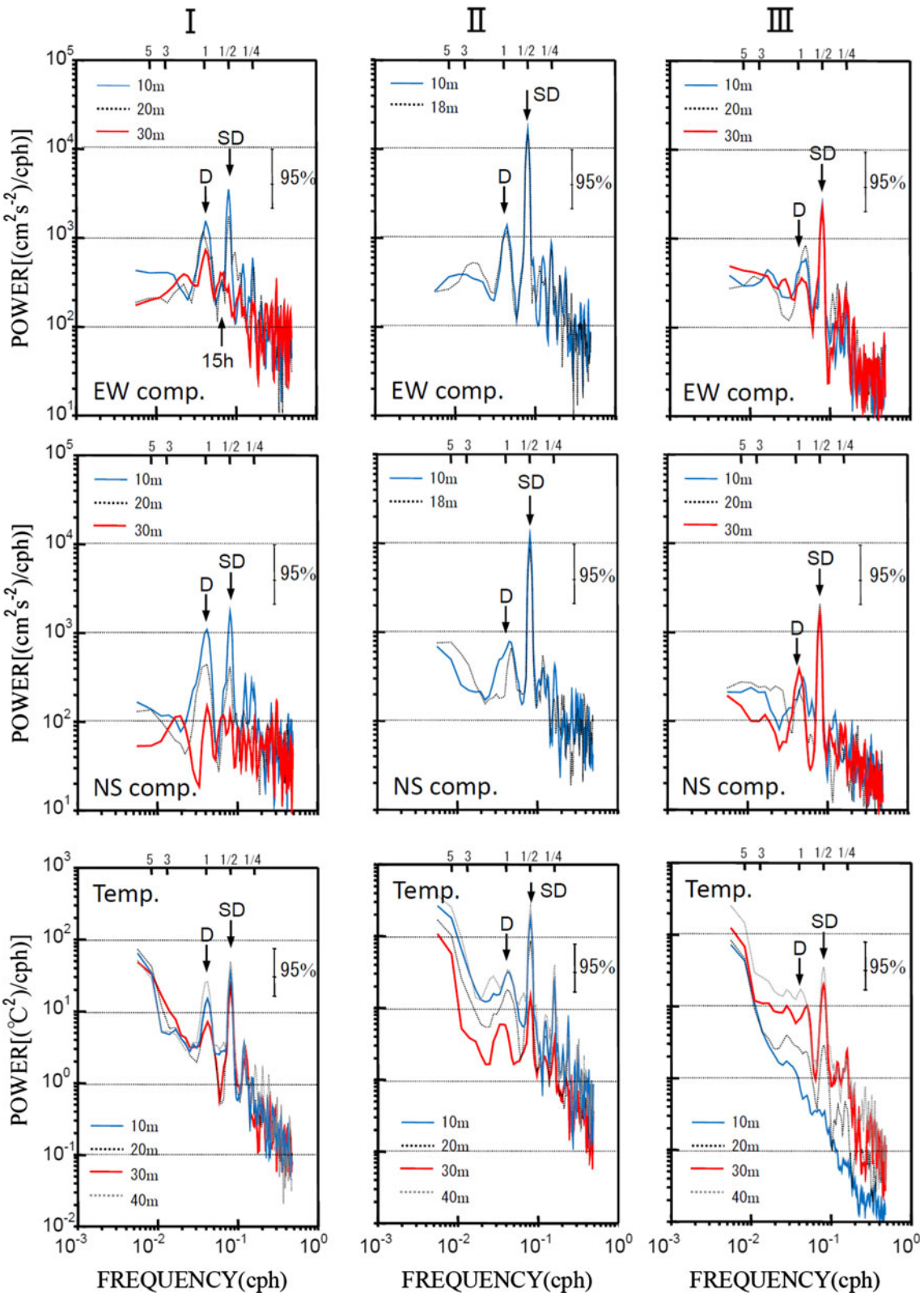

Fig. 5 Power spectra of eastward current (*upper panel*), northward current (*middle panel*) and temperature (*lower panel*) in each period. Period I: June 16–30; Period II: September 1–15; Period III: November 1–15

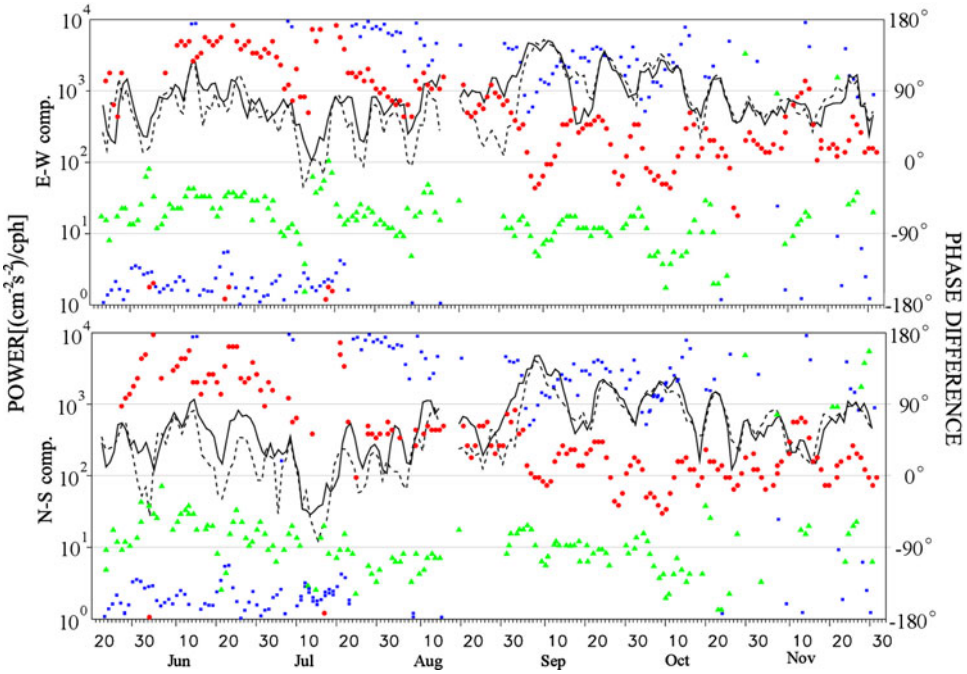

Fig. 6 Time variations of the energy level of semidiurnal period (12.4 h) for the eastward (*upper panel*) and the northward (*lower panel*) currents. *Solid line* 10 m, *dashed line* 18 m. *Symbols* indicate phase difference between current at 10 m depth and sea level, *closed circle*; current at 10 m depth and temperature at 30 m depth, *filled triangle*; and temperature at 30 m depth and sea level, *filled square*

about 200° in the early observations, about 160° from the end of July to mid-August, and about 90° in September.

Consequently, it is reasonable to consider that observed current fluctuations were mainly due to the internal tide.

4.3 Vertical current structure

One of the purposes of this study is to clarify the characteristics of current structure in the outer part of Tokyo Bay. Unfortunately, current data below 20 m depth were not obtained from the end of August to the middle of September. However, to describe the current structure before and after the maximum temperature period provides us with some good information about the internal tide in the study area. Although current oscillations were considered to mainly due to the internal tide from the phase relationship between sea surface and current, the horizontal current fluctuated at the same time in the vertical after the deepening of the thermocline from the middle September. In this study, we examined the vertical structure of the current using an empirical orthogonal function (EOF). Eigenfunctions and eigenvalues for the semidiurnal period band were calculated using a band-pass (8–16 h) filtered data. In the EOF analysis, two consecutive periods were selected: period A, June 1–July 15, and period B, October 1–November 15. Periods I and III in the previous section of spectral analysis were included in periods A and B, respectively.

Figure 7 shows the vertical structure of the EOF modes, and Table 1 presents the eigenvalue in each period. In period A, the first EOF mode shows that the amplitude decreases from surface to bottom and becomes zero near the bottom for the eastward component, but not for the northward component. Contributions of the first EOF mode for both components are more than 70%, and contributions of the second and third EOF modes also important. The second EOF mode, having a contribution of 16% of the eastward component, shows a structure similar to the first dynamical mode; that is, the current direction in the lower layer is opposite to that in the upper layer. In period B, the first EOF mode has a contribution of more than 90% for both eastward and northward components, and it shows a structure similar to a barotropic wave (amplitudes of the first EOF mode are almost the same in the vertical). Although the current oscillations are expected to be mainly due to the internal tide resulting from the phase relationship between the current and surface displacements, the vertical structure of the current interestingly exhibit a barotropic structure.

5 Discussion

5.1 Relationship of the current structure and internal tide

Observation and numerical models by Kitade and Matsuyama (1997) indicated that the semidiurnal internal tide observed in Sagami Bay is generated at the northern part of the Izu Ridge and the shallow region off Suno-saki, at the southwestern tip of Boso Peninsula. In this study, the internal tide observed in the outer part of Tokyo Bay

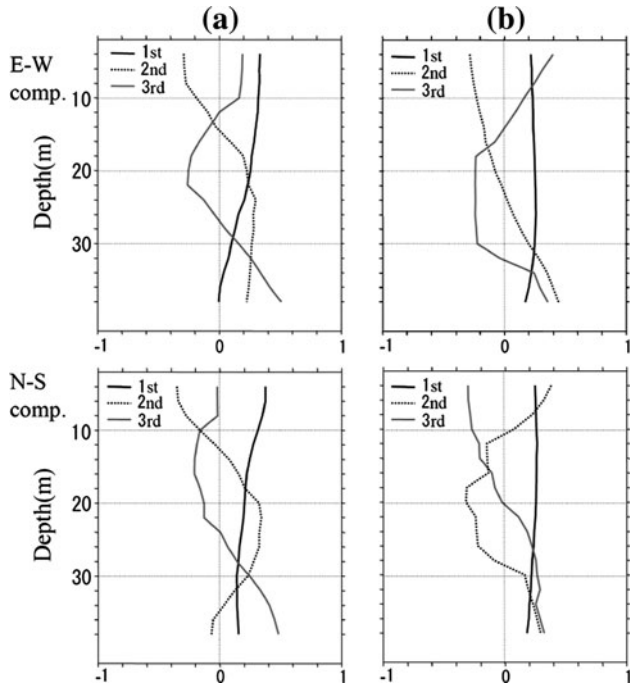

Fig. 7 Vertical structure of the lowest three EOF modes calculated from band-pass filtered data (from 8 to 16 h). Period *A*: from June 1 to July 15; period *B*: from October 1 to November 15

Table 1 Eigenvalues and their percentages for each EOF mode in periods A (June 1–July 15) and B (October 1–November 15)

	1st	2nd	3rd
A			
E–W	302.1 (71.2%)	70.4 (16.6%)	25.7 (6.1%)
N–S	161.4 (76.9%)	20.5 (9.8%)	12.4 (5.9%)
B			
E–W	813.9 (91.0%)	58.4 (6.5%)	10.9 (1.2%)
N–S	554.2 (94.3%)	16.9 (2.9%)	7.7 (1.3%)

appears to be generated in the shallow region off Sunosaki, and propagates into the study area. Since the higher-mode internal waves easily decay near the generation region, lower-mode internal waves are expected to propagate into the bay and reflect or scatter at the shelf edge. Kawamura and Kitade (2007) theoretically discussed reflection and scattering problems in the narrow shelf region and indicated that higher-mode internal waves are regenerated by the lowest-mode internal waves at the shelf edge to satisfy boundary conditions.

When the density stratification existed on the continental shelf in period A, the current structure of the first EOF mode showed baroclinicity for the eastward component, and contributions of the second and third EOF modes were crucial for both eastward and northward components. These results indicate that the higher mode internal waves were regenerated at the shelf edge and effects of their currents appeared in the observed data.

However, when the thermocline depth increased and the density became homogeneous on the shelf in period B, the current structure of the first EOF mode was similar to a barotropic tide with a contribution greater than 90% for both eastward and northward components (Table 1). While the current structure in period B was similar to a barotropic tide, the eigenvalue in period B was about three times greater than that in period A, indicating the strengthening of the semidiurnal tidal oscillation. The observed strong current with a barotropic structure cannot be explained by a surface tidal current, because there is no amplification mechanism for the surface tide in period B. Our sampling station was located about 3 km from the shelf edge. This distance is much shorter than the internal radius of the deformation, about 15 km, in the deep region of the outer part of Tokyo Bay. Thus, it is possible that the signal of internal tides propagating in the deep region appeared in the current data on the shelf edge.

5.2 Amplification of the semidiurnal internal tide

From the satellite images of NOAA/AVHRR (Fig. 8), warm water originating from the Kuroshio was found to intrude into the outer part of Tokyo Bay when the semidiurnal current oscillation was significantly amplified. The effect of the warm water intrusion was confirmed by sea level fluctuations at Mera and Miyake Island (Fig. 3b). Sea level at Miyake Island abruptly increased at the end of August. An abrupt temperature increase occurred during the same period when the sea level rose abruptly. Sea level variations at Miyake Island have been reported to correlate with the variation in the Kuroshio axis and surface circulation in Sagami Bay (Kawabe and Yoneno 1987; Iawata and Matsuyama 1989). The sea level rise at Miyake Island implies that the Kuroshio axis shifts to the north of that island. These results indicate that the deepening of the thermocline in the outer part of Tokyo Bay was induced by the warm water intrusion originating from the Kuroshio.

In some cases, amplification of a semidiurnal internal tide is due to the deepening of thermocline. Internal tides are primarily generated by surface tidal currents at a steep slope region, e.g., sea mounts and ridges (Rattray 1960; Baines 1973, 1982; Hibiya 1986). The vertical displacement of the internal tide is induced by the vertical current due to the surface tidal current over the topography. Such a vertical current is at a maximum near the sloping bottom, and it gradually decreases with height from the bottom (e.g., Baines 1982). Thus, the vertical displacement of the thermocline is at the maximum when the thermocline depth is deepened and near the sloping bottom. Efficient energy

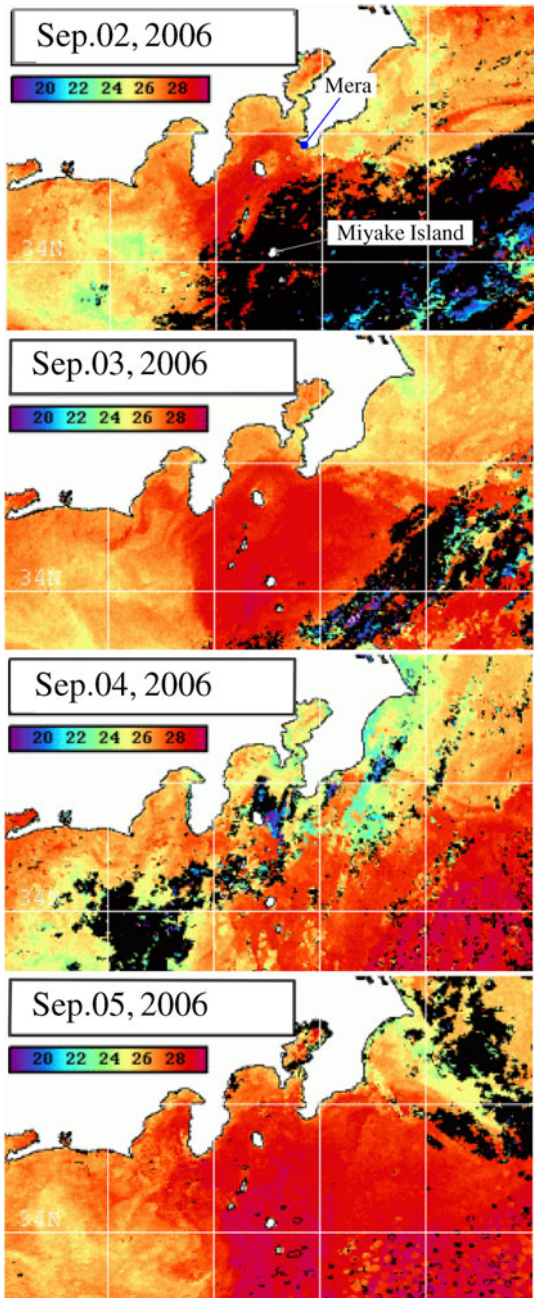

Fig. 8 AVHRR sea surface temperature composite images on 1 day from September 2 to 5, 2006

transformation from the surface tide to the internal tide is expected in the strongly stratified ocean. However, the effect of the efficient energy transformation cannot explain the significant amplification of the semidiurnal period in early September, because the energy level for the diurnal period, implying the amplitude of the diurnal internal tide, was not amplified in period II as shown in Fig. 5.

Next, we discuss the other amplification mechanism of the semidiurnal internal tide, i.e., due to the effect of reflection and interference. Spectral energy levels for the semidiurnal period bands in periods I and II are compared in Fig. 5. The energy peak of the semidiurnal period band in period II is single and clear, and its energy level is significantly higher than in the other periods. There are some small peaks in the semidiurnal period band at 30 m depth for both current components in period I, e.g., the peak at the 15-h period for the eastward current is slightly higher than at the 12-h period.

Phase difference between the temperature at 30 m depth and the current at 10 m depth were estimated for the semidiurnal constituent (Table 2). The eastward and northward currents in period I lead the temperature by 45° (1.5 h) and 60° (2 h), respectively. Both eastward and northward currents in period II lead the temperature by 90° (3 h), indicating the characteristics of a standing wave. The result that the property of a standing wave appeared when semidiurnal oscillation is large indicates a possibility that effective reflection and resonance is caused near the observational station.

Next, let us consider a possibility of resonance of semidiurnal internal tide; the phase speed, C, of the internal wave in the two layer ocean is:

$$C = \sqrt{\frac{\Delta\rho}{\rho} g \frac{h_1 h_2}{H}},$$

where $\Delta\rho$ is the density difference between the upper and lower layers, g (= 9.8 m s^{-2}) is the gravity, h_1 and h_2 are the thickness of the upper and lower layers, respectively, and H is the water depth. Here, a water depth of 500 m is selected because the effect of the internal wave in the deep region of the outer part of Tokyo Bay is being examined. When we assume $\Delta\rho/\rho = 0.0021$ and $h_1 = 30$ m for period I, the phase speed of the internal wave is $C = 0.76$ m s^{-1}. A canyon extends from north to south in the outer part of Tokyo Bay. Shallow regions exist on both the north and south sides of the canyon; the northern side is off Kannon-zaki and the southern side is a shallow region off Suno-saki. Considering an eigenmode with a fixed boundary on both sides, the internal seiche with half a wave length in the north–south distance of the canyon is expected to exist in this area. The north–south distance of the canyon is about 21 km, and the period of the internal seiche in the weak stratification period is about 15 h. On the other hand, if we assume $\Delta\rho/\rho = 0.0025$ and $h_1 = 40$ m for period II, then phase speed and the period of internal seiche are 0.95 m s^{-1} and 12.3 h, respectively. Thus, the period of internal seiche is close to the period of the M2 constituent (12.42 h). The result of this trial calculation of the internal seiche in the canyon explains the properties found in the spectral analysis, i.e., a small peak was found at the 15-h period in Period I and a single large peak was found at the semidiurnal period in Period II.

Table 2 Phase relations between each combination for the semidiurnal period

	Current–sea level		Current–temp.		Temp.–sea level (°)
	E–W comp. (°)	N–S comp. (°)	E–W comp. (°)	N–S comp. (°)	
Period I	145	124	−45	−60	−152
Period II	5	1	−91	−89	92

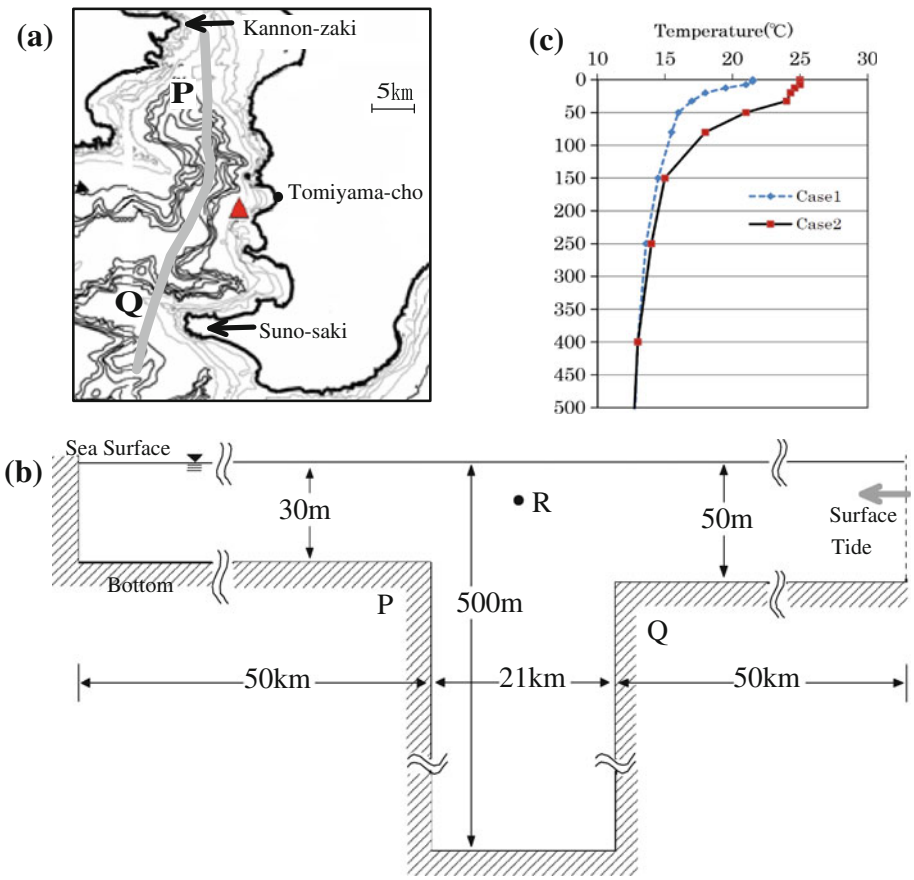

Fig. 9 **a** Bottom topography around deep canyon of outer part of Tokyo Bay. *Thick gray line* indicates the axis which idealized in the model domain. Points *P* and *Q* are shallow regions off Kannon-zaki and off Suno-saki, respectively. **b** Model domain idealized 2-dimensional model. Points *P* and *Q* correspond to shallow region shown in (**a**). **c** Vertical profile of temperature used in the model for Case 1 and Case 2

Consequently, it can be shown that the primary mechanism for amplification of the semidiurnal internal tide during a period of strong stratification is the resonance of the internal seiche and the semidiurnal internal tide. However, it is difficult to explain the observed phase relation between the current and sea level; that is, the surface current is almost in phase with the surface displacement in the coastal region, as shown in Table 2. The phase relation will be explained in the following section.

5.3 Amplification mechanism using a numerical model assuming a simplified topography

The following are the observed phase relationships between the water current and sea level for the semidiurnal period: (1) the surface displacement leads the surface current by about 124° in a weak stratification period and (2) the fluctuations in both current and surface displacement are almost in phase in a strong stratification period. This section discusses the resonance of the internal seiche and semidiurnal internal tide and examines the phase relationship of sea level and surface current using a two-dimensional model assuming a simplified topography.

5.3.1 Model

The deep narrow canyon in the outer part of Tokyo Bay meanders as shown in Fig. 9a. The wave property in such a narrow canyon must have a characteristic of an internal Kelvin wave because the internal radius of deformation is much larger than the width of the canyon, as discussed by Webb and Pond (1986). Thus, in this study, the property of

the internal wave along the thick gray line in the figure was examined by two-dimensional level model. A side view of the model is shown in Fig. 9b. In the model domain, the deep canyon is shown as 500 m deep and 21 km length. The inner part of Tokyo Bay is shown on the left of the model domain by 50 km length and 30 m deep, and the shallow region off Suno-saki is expressed on the right as 50 m deep. Points P and Q in the real topography correspond to the shallow steps P and Q in the model domain. The grid size is 1 km horizontally, and the grid points are set at constant depth in z level, that is, ten vertical levels were set at depths of 2.5, 7.5, 12.5, 20, 32.5, 50, 80, 150, 250, 400 m. Other parameters and basic equations used in the model are the same as those used in the model of Igeta et al. (2009).

In this numerical model, surface elevation at a period of 12 h and amplitude of 0.3 m were given the open boundary (dashed line in Fig. 9b) and the generation of the semidiurnal internal tide and its interaction with the internal seiche in the model domain were examined. The initial conditions applied to the model used only temperature stratification. Case 1 exhibits weak stratification in June, and Case 2 exhibits strong stratification in the early September (Fig. 9c). Salinity is assumed to be homogeneous in both cases.

5.3.2 Result

Figure 10 shows the time variations of the surface displacement and the vertically averaged current (barotropic tidal current) at Q, and the current at R (10 m depth in the center of the deep region as shown in Fig. 9b). In this figure, positive values indicate the current toward the head of the bay (at the left in Fig. 9b). The current at 10 m depth was not very strong in Case 1, whereas the current amplified gradually with time and its amplitude reached 40 cm s^{-1} in Case 2.

Next, we focus on the phase relationships. The barotropic tidal current always leads the sea level displacement by 90° in both Case 1 and Case 2, indicating a characteristic of a standing wave in the coastal region. The phase relationship between the current and sea level displacement changes significantly in these two cases. While the sea level displacement leads the current at 10 m depth by about 120° in Case 1, in Case 2, both the sea level displacement and current are in phase. These phase relationships agreed well with the observed results.

Here, we explain the amplification process and phase relationship from the vertical distribution of temperature and current around the deep region (Fig. 11). The insets show sea level and surface tidal current which was estimated as the vertically averaged current at Q. Since the surface tide has a characteristic of a standing wave in the model domain, the surface tidal current fluctuates almost in

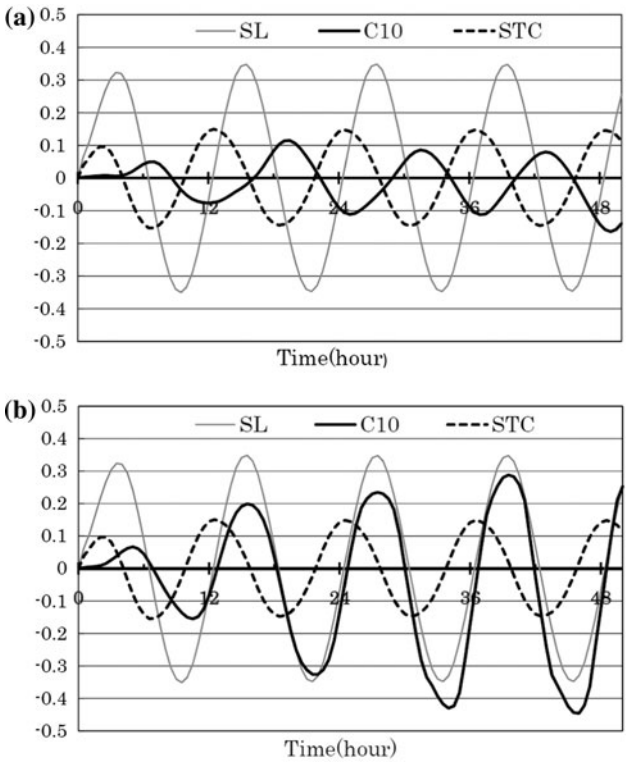

Fig. 10 Time variations of sea level, surface tidal current and current at 10 m depth for the stratification condition of Case 1 (**a**) and Case 2 (**b**). *SL* sea level over the shallow region Q in Fig. 9b (cm), *STC* Surface tidal current over the shallow region at Q in Fig. 9b (cm s^{-1}), *C10* current at R in Fig. 9b (cm s^{-1})

phase throughout the model domain. Forcing from the surface tide tothe internal tide over the abrupt change in topography is proportional to the strength of the vertical component of the surface tidal current. At $t = 36$ h, the surface tidal current toward the bay head is at a maximum during the period of flood tide and the thermocline is depressed by downward forcing induced by the surface tidal current around Q. At the same time, the rise of the thermocline is also induced around P by upward forcing. The thermocline depression generated around Q propagates to the north at $t = 37.5$ h and its front reaches the northern end of deep region (around P) at $t = 39$ h. At $t = 40.5$ h, the surface tide is in the phase of ebb tide and the surface tidal current changes to the south. At this time, the thermocline depression reached around P is reinforced by downward forcing again. The thermocline depression is amplified during the period of ebb tide (from $t = 40.5$ to 43.5 h). On the other hand, the thermocline rise generated by the upward forcing around P at $t = 36$ h propagates to the south and is also reinforced around Q during the period of ebb tide. Since the thermocline rise can propagate over the shallow region, that is, a part of energy of the oscillation leaks over the shallow region, the front of the thermocline rise is not so clearly seen in the deep region in

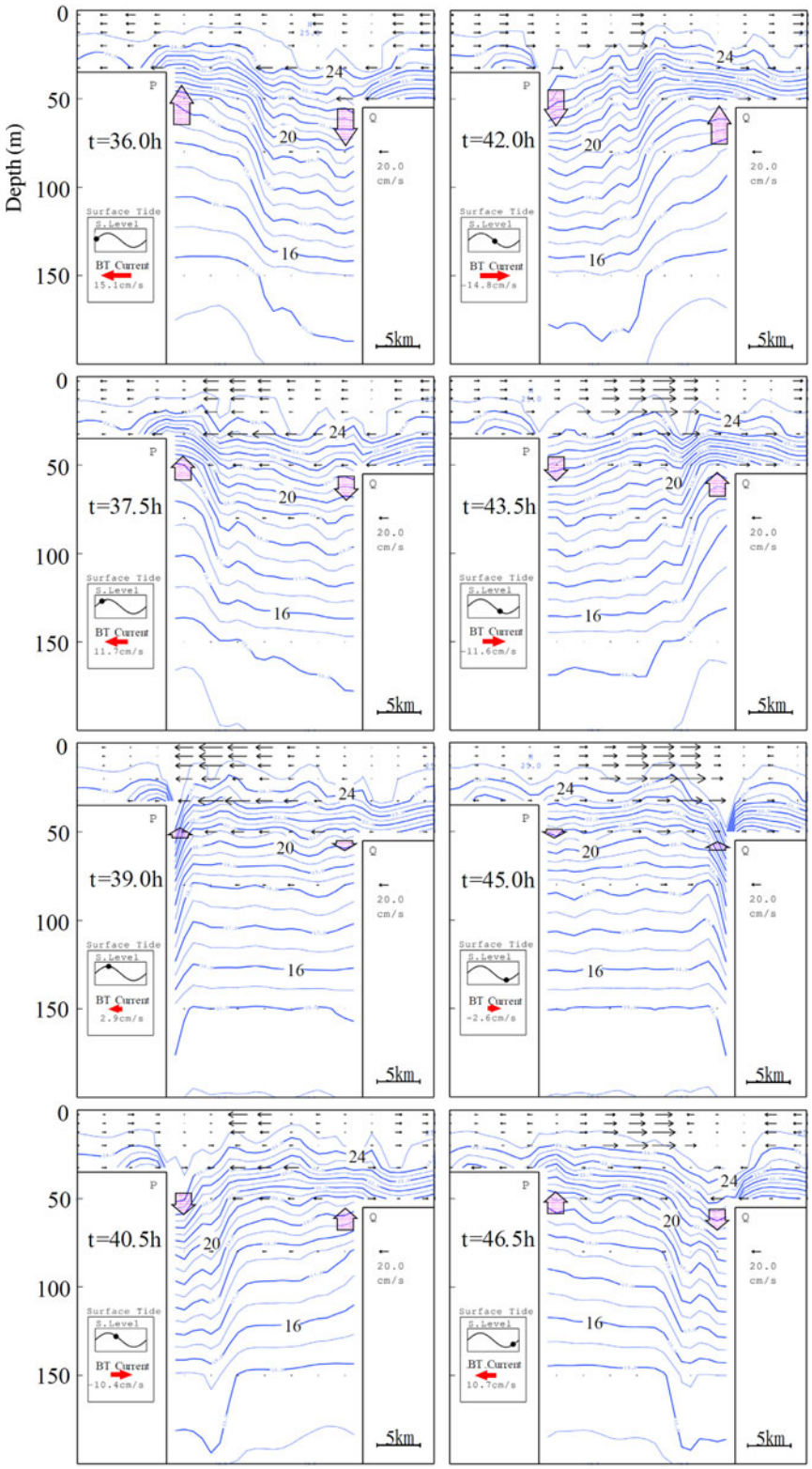

Fig. 11 Distributions of temperature contour lines and current vectors aroundthe deep canyon region in Case 2. States of surface tide, i.e., sea level and surface tidal current (*BT current* barotropic tidal current) at Q in Fig. 9b, are indicated at *left bottom* of each figure. *Wide arrow* indicates forcing induced by the surface tidal current over the abrupt change in topography

this model condition. In this way, the internal tide is resonantly generated in the deep region, when the period of internal seiche in the deep region is nearly semidiurnal. Thus, the currents associated with the internal tide are also amplified and strong currents appear in the upper layer near the center of the deep region.

Consequently, using a simplified topographic model, the amplification mechanism of the semidiurnal current

oscillation and the phase relationship observed in the early September were well explained. The generated strong current would induce strong mixing in the outer part of Tokyo Bay in the area having irregular bottom topography.

6 Summary

To investigate the dynamic properties in the outer part of Tokyo Bay, monitoring observations using a thermistor array and an acoustic Doppler current profiler were carried out at the mouth of Tokyo Bay from May 20 to November 30, 2006. During the maximum temperature periods in early September, the current fluctuations with the tidal periods were significantly amplified. The strong currents made the use of set nets for fishing difficult. While the current fluctuation was believed to be related to the baroclinic motion on the basis of phase relationsships among temperature, current, and sea level fluctuations, the vertical structure of the EOF mode showed the dominance of the barotropic structure. Such a discrepancy of current structure was explained by considering the effect of an internal tide propagating in the deep region at the mouth of Tokyo Bay. Furthermore, we have indicated that amplification of the semidiurnal internal tide and warming of the temperature field were caused by the intrusion of Kuroshio warm water. The amplification mechanism of the semidiurnal internal tide was examined using a two-dimensional model with simplified bottom topography. The results revealed that the semidiurnal internal tide was resonantly generated in the deep canyon at the mouth of Tokyo Bay when the stratification becomes strong and the period of the internal seiche approaches that of the semidiurnal tide. The observed phase relationsships were also well explained by the model.

Acknowledgments We wish to thank Mr. H. Hamada and Mr. K. Matsumoto of Nitiyu Giken Kogyo Co., Ltd., for their help in carrying out the observations. We also thank the captain and crew of the fisheries boat for their help in the observations. Sea level data were obtained from the Japan Oceanographic Data Center. Barometric data and wind data were obtained from the Japan Meteorological Agency. We would like to thank both agencies for their help. Monitoring during this study was made possible with the help of a subsidy from the Nippon Foundation.

References

Baines PG (1973) The generation of internal tides by flat-bump topography. Deep Sea Res 20:179–205

Baines PG (1982) On internal tide generation models. Deep Sea Res 29:307–338

Fujiwara T, Yamada Y (2002) Inflow of oceanic water into a coastal embayment (Tokyo Bay) and generation of subsurface hypoxic water mass. J Geophys Res 107:C513110. doi:10.1029/2000JC000749

Guo X, Yanagi T (1998) Variation of residual current in Tokyo Bay due to increase of fresh water discharge. Cont Shelf Res 18:677–693

Hibiya T (1986) Generation mechanism of internal waves by tidal flow over a sill. J Geophys Res 91:7697–7708

Igeta Y, Kumaki Y, Kitade Y, Senjyu T, Yamada H, Watanabe T, Katoh O, Matsuyama M (2009) Scattering of near-inertial internal waves along the Japanese coast of the Japan Sea. J Geophys Res 114:C10002. doi:10.1029/2009JC005305

Ishidoya H, Kitade Y, Matsuyama M, Iwata S, Ishii M, Igeta Y (2006) The Kyucho current in Sagami Bay and at the mouth of Tokyo Bay induced by the eastward propagation of small meanders of the Kuroshio. Umi no Kenkyu 15:235–247 (in Japanese with English abstract)

Iwata S, Matsuyama M (1989) Surface circulation in Sagami Bay: the response to variations of the Kuroshio axis. J Oceanogr Soc Jpn 45:310–320

Kawabe M, Yoneno M (1987) Water and flow variations in Sagami Bay under the influence of the Kuroshio path. J Oceanogr Soc Jpn 43:283–294

Kawamura Y, Kitade Y (2007) Effects of scattering and resonance on energy dissipation of internal tide in narrow shelf. J Oceanogr 63:15–25

Kitade Y, Matsuyama M (1997) Characteristics of internal tides in the upper layer of Sagami Bay. J Oceanogr 53:143–159

Kitade Y, Matsuyama M (2000) Coastal-trapped waves with several-day period caused by wind along the southeast coast of Honshu. Jpn J Oceanogr 56:727–744

Matsuyama M, Iwata S (1985) Semidiurnal internal tides observed over the continental shelf off Jyogashima in Sagami Bay. J Tokyo Univ Fish 72:43–49 (in Japanese)

Matsuyama M, Iwata S, Maeda A, Suzuki T (1992) Kyucho in Sagami Bay. Bull Coastal Oceanogr 30:4–15 (in Japanese)

Ohwaki A, Matsuyama M, Nagashima H (1994) Difference in the predominance of internal tidal currents in Sagami and Suruga Bays. J Oceanogr Soc Jpn 47:194–206

Radjawane IM, Matsuyama M, Kitade Y, Suzuki T (2001) Numerical modeling of density-driven current in Tokyo Bay. La Mer 36:63–75

Rattray M Jr (1960) On the coastal generation of internal tides. Tellus 12:54–62

Webb AJ, Pond S (1986) A modal decomposition of the internal tide in a deep, strongly stratified inlet: knight inlet, British Columbia. J Geophys Res 91:9721–9738